Nanoscale

Accepted Manuscript

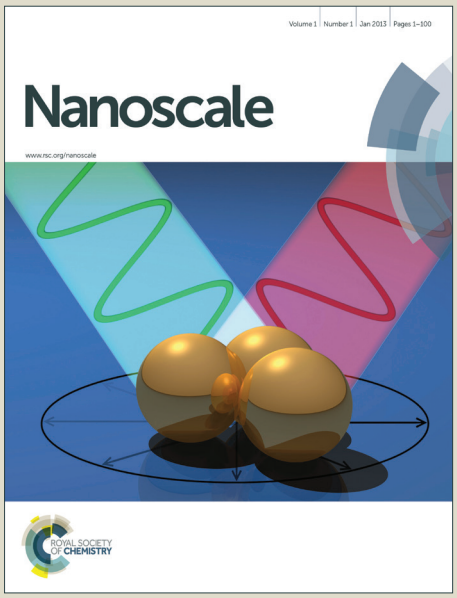

General synthesis of noble metal (Au, Ag, Pd, Pt) nanocrystals modified MoS_2 nanosheets and enhanced catalytic activity of Pd-MoS_2 for methanol oxidation

Lihui Yuwen,[a] Fei Xu,[a] Bing Xue,[a] Zhimin Luo,[a] Qi Zhang,[a] Biqing Bao,[a] Shao Su,[a] Lixing Weng,[b] Wei Huang,*[a] and Lianhui Wang*[a]

Received (in XXX, XXX) Xth XXXXXXXXX 20XX, Accepted Xth XXXXXXXXX 20XX
DOI: 10.1039/b000000x

A general and facile method for water-dispersed noble metal (Au, Ag, Pd, Pt) nanocrystals modified MoS_2 nanosheets (NM-MoS_2 NSs) has been developed. By using sodium carboxymethyl cellulose as stabilizer, well-dispersed NM-MoS_2 NSs with homogeneously deposited noble metal nanocrystals (NM NCs) can be synthesized in aqueous solutions. Due to the transition from semiconducting 2H to metallic 1T phase, the chemically exfoliated MoS_2 (ce-MoS_2) NSs have improved electrochemical activity. The partially metallic nature of ce-MoS_2 NSs and catalytic activity of NM NCs synergistically make NM-MoS_2 NSs potential electrochemical catalyst. For the first time, Pd-MoS_2 NSs was used as electrocatalyst for methanol oxidation in alkaline media. The results showed that Pd-MoS_2 NSs have enhanced catalytic activity with 2.8-fold anodic peak current mass density compared to commercial Pd/C catalyst, suggesting potential application for direct methanol fuel cells (DMFCs).

Introduction

Since the successful preparation of free-standing single-layer graphene in 2004, two-dimensional (2D) nanomaterials have drawn great attention due to their unique structure and distinctive properties compared with their bulk forms, which opens the door to a novel world for physics, chemistry, biomedicine, and many others.[1-2]

Considered as novel inorganic graphene analogues, layered transition metal dichalcogenides (LTMDs) have become a new focus during recent years.[3-6] LTMDs with generalized formula of MX_2 include a large family of compounds, where M is 4B, 5B, or 6B transition metals, and X is sulfur, selenium, or tellurium, such as VS_2, $NbSe_2$, TaS_2, MoS_2, WTe_2, TiS_2, $ZrSe_2$.[4, 6-7] These compounds have unique 2D X-M-X structure in which the transition metal atom layer is sandwiched between two close-packed chalcogen atom layers. Within the LTMDs layer, transition metal atoms and chalcogen atoms form strong covalent bonds, while between the layers weak van der Waals force is the main interaction.[7]

As a prototypical compound of LTMDs, MoS_2 has been extensively studied as solid lubricant, hydrodesulphurization catalyst, hydrogen evolution catalyst, and optoelectronic materials.[8-11] Bulk MoS_2 is a typical semiconductor with an indirect band gap about 1.2 eV.[12-13] However, when the thickness of MoS_2 crystals decreases to single-layer, the band gap transforms from indirect to direct type due to quantum confinement effect in their d-electron system.[14] The structure alternation of single-layer MoS_2 nanosheets (MoS_2 NSs) to their bulk ones leads to intriguing optical and electrical properties. For example，Heinz and Wang found that single-layer MoS_2 NSs can emit strong photoluminescence both from theoretical analysis and experiments, which not only provides the first sample of atomic-thin photoluminescent nanomaterials but also suggests potential applications for optical sensing, photocatalysis, and photovoltaics.[14-1518, 19] Kis et al. showed that single-layer MoS_2 NSs can be used to fabricate high performance field-effect transistors (FETs) and ultrasensitive photodetectors.[16-17]

Several methods have been developed to prepare ultrathin MoS_2 NSs, including mechanical exfoliation ("Scotch tape method"), liquid exfoliation, chemical vapor deposition (CVD), colloidal synthesis, chemical exfoliation (lithium intercalation-exfoliation), and electrochemical exfoliation.[18-26] Among these methods, chemical exfoliation is not only relative simple and reliable, but also capable for large scale preparation of single-layer nanosheets. Most interesting, while MoS_2 NSs obtained from other methods are usually semiconducting 2H phase, chemically exfoliated MoS_2 (ce-MoS_2) NSs are mainly metallic 1T phase.[27-28] Although the ce-MoS_2 NSs are not favourable for optoelectronic devices, such as FETs, they are quiet attractive for electrochemical catalysis. Very recently, Lukowski et al. demonstrated the ce-MoS_2 NSs can significantly improve the hydrogen evolution reaction (HER) catalytic performance with high electrocatalytic current density and low overpotentials due to the existence of metallic 1T phase.[29] Voiry et al. reported similar results that ce-WS_2 NSs can also be used as excellent HER catalyst due to the presence of high concentration of the strained metallic 1T phase.[30] Hence, chemical exfoliation method not only provides a facile way to prepare ultrathin MoS_2 NSs but also produces novel materials with the same composition yet significantly improved electrical properties, which offers novel opportunities for HER and even more other electrocatalytic applications.

On the other hand, noble metal (such as Au, Ag, Pt, Pd) nanocrystals (NM NCs) are another prototypical functional nanomaterials with zero-dimensional (0D).[31-32] Modifying 2D nanomaterials with 0D NM NCs to form 0D-2D functional hybrids not only enhances the intrinsic properties of the materials, but also bring novel properties and functions. For example, the noble metal-graphene hybrids have been widely used as optical biosensors and advanced electrocatalysts for energy conversion.[33-35]

Recently, several groups reported the preparation of NM NCs modified MoS_2 NSs. Rao et al. synthesized few-layer MoS_2 NSs by hydrothermal method and decorated the as-prepared LTMDs NSs with Au, Ag, and Pt.[36] However, this method needs very

high temperature (773 K) and has trouble to control the thickness of MoS_2 NSs. Zhang et al. reported the epitaxial growth of Pd, Pt, and Ag NCs on the surface of single-layer MoS_2 NSs prepared by electrochemical exfoliation and showed that Pt-MoS_2 NSs exhibits high catalytic activity for HER.[37] Although electrochemical exfoliation is a very effective method to prepare single-layer MoS_2 NSs, bulk MoS_2 need to be intercalated in a Li-battery system, which is relative complicated to assembly and not easy to scale up. Kim et al. decorated ce-MoS_2 NSs with Au NCs by directly reducing Au(III) cations with MoS_2 NSs and the resulting Au-MoS_2 NSs show significantly enhanced electrocatalytic performance toward HER.[38] Although this method is very simple, lacking stabilizer often leads to aggregations of the products.

Herein, we develop a general, facile, and scalable method to prepare water-dispersible noble metal NCs modified ce-MoS_2 NSs (NM-MoS_2 NSs, NM=Au, Ag, Pd, Pt) by using carboxymethyl cellulose as stabilizer in aqueous solution. Structure and optical properties of the NM-MoS_2 NSs were characterized and the electrocatalytic activity of Pd-MoS_2 NSs for methanol oxidation in alkaline solutions was also studied.

Experimental Section

Chemicals

Molybdenum (IV) sulphide (MoS_2) powder (<2 μm, 99%) and Pd/C (10 wt%) were purchased from Sigma-Aldrich; n-butyllithium (n-BuLi, 2.4 M hexane solution) was bought from Amethyst; sodium carboxymethyl cellulose (CMC, 800-1200 mPa·s), Tween 80, sodium dodecyl sulfate (SDS), cetyl trimethyl ammonium bromide (CTAB), acetone, isopropanol, alcohol, ascorbic acid (AA), $HAuCl_4{\cdot}4H_2O$, $AgNO_3$, $H_2PtCl_6{\cdot}6H_2O$, and $PdCl_2$ are all analytical grade, purchased from Aladdin, China. Ultrapure water (18.2 MΩ, Millipore) was used to prepare aqueous solutions in all of the experiments.

Synthesis of MoS_2 NSs by lithium intercalation-exfoliation

Ultrathin MoS_2 NSs were prepared by lithium intercalation and exfoliation method first reported by Joensen et al. with some modifications.[20] In a typical experiment, 0.8 g MoS_2 was added into a 50 ml Schlenk tube under Ar atmosphere, followed the addition of 25 mL n-BuLi hexane solution. The mixture was stirred at room temperature for 48 h and then allowed to settle for hours. The supernatant of the mixture was removed and the residual black solid was collected. Then Ar-saturated water was carefully introduced into the tube to avoid sputtering under the protection of Ar, since copious hydrogen gas releases at the moment. The ce-MoS_2 NSs aqueous suspension was sonicated for 1 h to complete the exfoliation process and then centrifuged at 1500 rpm for 20 min. After centrifugation, the precipitates were discarded and the supernatant was centrifuged at 10000 rpm for 30 min. The black slurry was redispersed in water and centrifugated again until the aqueous dispersion reached neutral.

Synthesis of NM-MoS_2 NSs (NM=Au, Ag, Pd, and Pt)

For Au-MoS_2 NSs synthesis, 3 ml（0.05 mg/ml）MoS_2 NSs aqueous dispersion was added into a 10 mL quartz tube equipped with a magnetic bar. Under stirring, 50 μL AA aqueous solution (100 mM), 10 μl CMC aqueous solution (100 mM), and 10 μL $HAuCl_4$ aqueous solution (48.5 mM) were mixed with MoS_2 NSs aqueous dispersions. The reaction mixture was then heated at 60 □ for 5 min with microwave irradiation using a CEM microwave system (Discover Application Software Version 3.5.7, CEM, USA).

Other NM-MoS_2 NSs can be synthesized according to the similar procedure, while $HAuCl_4$ was changed to $AgNO_3$, $H_2PtCl_6{\cdot}6H_2O$, and $PdCl_2$, respectively.

Characterization

UV-vis-NIR adsorption spectra were measured on a Shimadzu UV-3600 spectrophotometer. Transmission electron microscope (TEM) images were taken on a Hitachi H-7500 electron microscope (120 kV) and High resolution TEM (HRTEM) characterization was performed on a Tecnai G2 F20 S-Twin electron microscope (200 kV) equipped with an energy dispersive X-ray spectrometer (EDS). Before TEM test, samples were purified by centrifugation for several times and then deposited onto the ultrathin carbon-coated copper grids (400 mesh, Zhongjingkeyi, China). The powder X-ray diffraction (XRD) was characterized on a D/max-γB diffractometer. Zeta potential data was obtained from ZetaPALS (Brookhaven, USA). X-ray photoelectron spectra (XPS) were performed on an PHI 5000 VersaProbe with Al Kα as the excitation source. The concentrations of MoS_2 and Pd were determined by Inductively Coupled Plasma Optical Emission Spectrometer (ICP-OES, Optima 5300 DV, PE).

Electrochemical measurements

All of the electrochemical measurements were performed on an Autolab PGSTAT302 (Metrohm China Ltd, Switzerland) electrochemical workstation with conventional three-electrode system.

Glassy carbon electrodes (GCEs) covered with ce-MoS_2 NSs, NM-MoS_2 NSs, or commercial Pd/C catalyst were used as the working electrode. Platinum wire and saturated calomel electrode (SCE) were used as the counter and reference electrodes, respectively. Before coating with different materials, the GCE was first polished with 1.0, 0.3, and 0.05 μm alumina powders and rinsed with ultrapure water, followed by sonication in acetone, alcohol, isopropanol, and ultrapure water, sequentially. Finally, the GCEs were dried under continuous nitrogen stream.

For cyclic voltammetry (CV) measurements of methanol oxidation, 7 μL aqueous suspensions of Pd-MoS_2 NSs and Pd/C catalyst with identical Pd concentration (35.2 mg/L) were deposited onto the cleaned GCE surface and then dried in the air for 8 hours at room temperature. Prior to catalytic activity study of methanol oxidation, the electrolyte solutions containing 0.5 M KOH and 1 M methanol were deaerated with N_2 bubbling for 30 min and N_2 atmosphere was kept over the solution during the electrochemical measurements. The CV measurements were performed at the potential range from -0.9 to 0.3 V *vs.* SCE at scanning rate of 100 mV/s .

In order to study the electrochemical properties of Pd-MoS_2 NSs before and after annealing, 20 μL aqueous suspensions of Pd-MoS_2 NSs were deposited onto ITO electrodes and dried in the air at room temperature. Then the ITO electrodes were annealed in Ar atmosphere at 300 □ for 1 hour before CV characterization and EIS test.

Results and discussion

Generally, the synthetic procedure involves three steps, as shown in Scheme 1: (1) Lithium intercalation of bulk MoS_2 to form Li_xMoS_2; (2) Exfoliation of Li_xMoS_2 to single or few-layer MoS_2 NSs; (3) Surface modification of MoS_2 NSs by noble metal NCs. The aim of the first two steps is to prepare water-dispersible thin MoS_2 NSs.

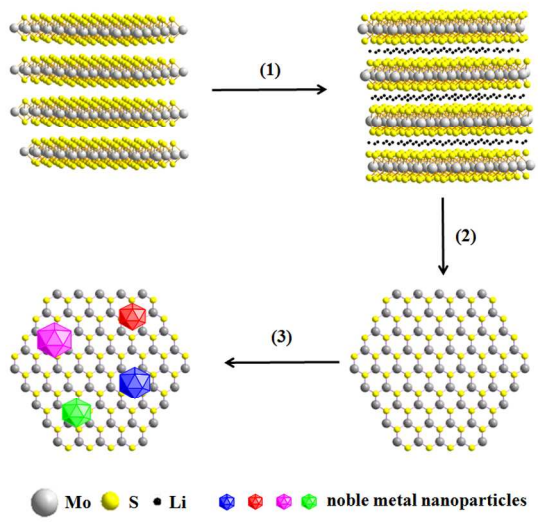

Scheme 1. The synthetic procedure of NM-MoS_2 NSs. (1) Lithium intercalation of bulk MoS_2; (2) Exfoliation of Li intercalated MoS_2 (Li_xMoS_2) to water-dispersable ce-MoS_2 NSs; (3) Noble metal nanocrystals deposition on the surface of ce-MoS_2 NSs to form NM-MoS_2 NSs.

As we know, there are several other methods for MoS_2 NSs preparation aside from chemical exfoliation, but each has its own drawbacks: The mechanical exfoliation has been successfully used to prepare high quality single-layer MoS_2 NSs, but it is time-consuming manual work and hard to scale up;[16] The liquid exfoliation assisted with sonication has been proven useful for numerous layered materials, but the products are usually flakes rather than single or few-layer nanosheets;[19] The electrochemical exfoliation is an effective and controllable method, but the lithium intercalation process need to be performed in lithium ion battery, which is complicated and only small amount of MoS_2 NSs can be prepared at a time (several milligrams level).[21] In contrast, chemical exfoliation is more simple, scalable, and has been proven reliable to prepare water-dispersible single-layer MoS_2 NSs.[20, 28] Under room temperature, n-BuLi can intercalate bulk MoS_2 with lithium atoms and form Li_xMoS_2 ($0<x<1$) in gram scale or more.[39] Li_xMoS_2 can then react with H_2O rapidly and release large amount of hydrogen gas, which can push the MoS_2 layers to separate with each other and form homogeneous ultrathin MoS_2 NSs. The third step of the synthetic procedure is to modify the MoS_2 NSs with noble metal NCs. In order to avoid the aggregation of noble metal NCs and MoS_2 NSs during preparation, appropriate stabilizer should be used. In this study we chose sodium carboxymethyl cellulose (CMC) as the stabilizer, since CMC has carboxyl modified polysaccharide structure with good water solubility and has been proven efficient stabilizer both for noble metal NCs and graphene nanosheets in aqueous dispersions.[40-45]

Fig. 1a shows the UV-vis-NIR absorption spectra of ce-MoS_2 NSs and NM-MoS_2 NSs aqueous dispersions. There are two absorption shoulder peaks in the visible region for ce-MoS_2 NSs: one is located at about 600 nm, which is associated with the transition from *K* point of the Brillouin zone; the other absorption peak near 400 nm can be assigned to the direct transition from deep valence band to the conduction band.[46] Compared with 2H-MoS_2, the excitonic features of the two peaks are relative weak, which is due to the lithium intercalation induced lattice distortion and phase transition from 2H to 1T.[28] After noble metal NCs modification, the absorption peaks changes significantly. For Au-MoS_2 NSs, the absorption peak at about 400 nm changes little, while the absorbance from about 500 nm to 1200 nm increases, which can be attributed the coupling of surface plasmon resonance (SPR) of the nearby Au NCs on the surface of MoS_2 NSs. Similarly, the wide absorption peak beyond 400 nm is the SPR peak of Ag NCs.[47] Both for Pd and Pt NCs modified MoS_2 NSs, no obvious new peaks emerge but the absorbance from 300 nm to 1200 nm increases obviously, since Pd and Pt NCs have wide absorption but no distinct absorption peaks in the UV-vis-NIR range.[48-49] Fig. 1b shows the zeta potential of ce-MoS_2 NSs and NM-MoS_2 NSs aqueous dispersions. Before NM NCs modification, zeta potential of ce-MoS_2 NSs is about -39 mV; after modification, the zeta potential of NM-MoS_2 NSs still remain in the range of -45 to -33 mV, indicating that NM-MoS_2 NSs have adequate negative charges on their surface with good colloidal stability.

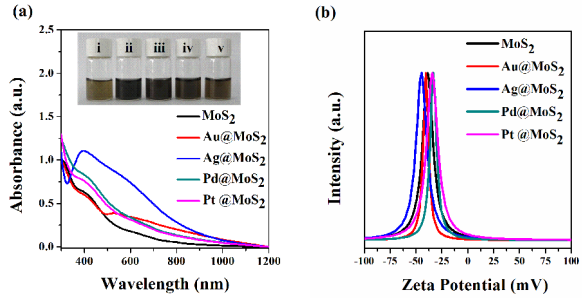

Fig. 1 (a) UV-vis-NIR absorption spectra and photographs (inset, from i to v) of ce-MoS_2, Au-MoS_2, Ag-MoS_2, Pd-MoS_2, and Pt-MoS_2 NSs aqueous dispersions; (b) Zeta potential analysis of ce-MoS_2 and NM-MoS_2 NSs.

The morphology and structure of ce-MoS_2 NSs and NM-MoS_2 NSs were studied by TEM and HRTEM characterization. As shown in Fig. 2a, bendings and foldings can be clearly observed from the basal plane of ce-MoS_2 NSs, which indicates that the ce-MoS_2 are very thin nanosheets. The lateral dimensions of MoS_2 NSs are usually in 200-1000 nm range (Figure S1, ESI). HRTEM image in Fig. 2b shows typical hexagonal single crystal structure of MoS_2 with distance of 0.271 nm for (100) Mo atoms.[21] The six folded SAED pattern in Fig. 2c indicates the MoS_2 NSs have single crystal structure with hexagonal symmetry.[28] After the reduction of $HAuCl_4$ by ascorbic acid, Au NCs formed and spreaded on the whole surface of MoS_2 NSs homogeneously, which can be seen from Fig. 2d. As shown in Fig. 2e, Au NCs grown on the surface of MoS_2 NSs are single crystal structure and the lattice spacing of 0.234 nm can be assigned to (111) plane of Au (JCPDS No. 89-3697). The formation of Au NCs on MoS_2

NSs has also been confirmed by EDS with the emergence of Au and Mo elemental peaks, as shown in Fig. 2f.

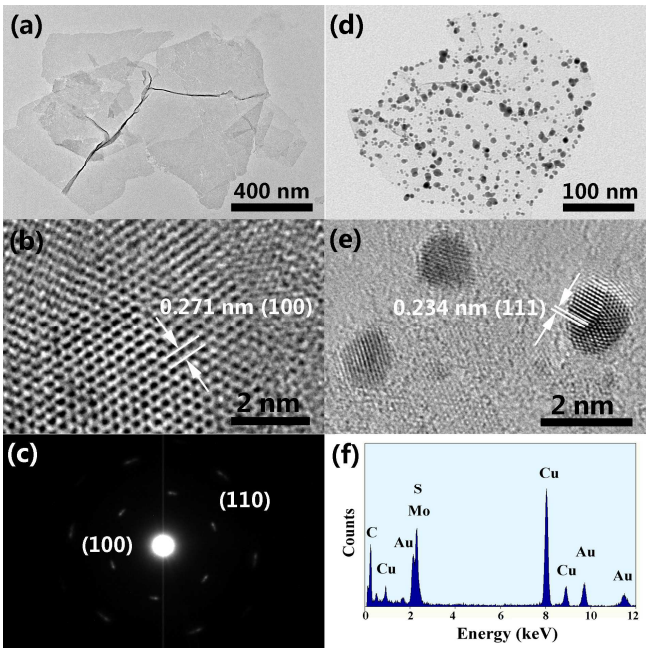

Fig. 2 TEM (a) and HRTEM (b) images of ce-MoS_2 NSs; (c) Selected area electron diffraction (SAED) pattern of ce-MoS_2 NSs; (d) TEM and (e) HRTEM images of Au-MoS_2 NSs; (f) Energy dispersive X-ray spectroscopy (EDS) of Au-MoS_2 NSs.

For the synthesis of water-dispersible NM-MoS_2 NSs, CMC played an important role as stabilizer. Rich carboxyl and hydroxyl groups of CMC can interact with noble metal atoms and assist the NM NCs to homogeneously deposit on the surface of MoS_2 NSs; Moreover, CMC can supply enough electrostatic repulsion force and steric hindrance to render NM-MoS_2 NSs with good stability. As shown in Figure S2, when Tween 80 was used as the stabilizer instead of CMC under the same experimental conditions, NM NCs prefer to form at the edges of MoS_2 NSs, which is similar to the Au-MoS_2 NSs prepared without stabilizers.[38, 50] The selective growth phenomenon may originate from that Tween 80 has no ionic groups as anchoring sites and the metal atoms tend to absorb onto the defect-rich edge sites with high surface energy[51]. Other small molecular surfactants, such as SDS, CTAB, have also been tried for NM-MoS_2 NSs synthesis, however, the products have relative weak colloidal stability and tend to form large aggregations.

In order to show the generality of this method, other noble metal modified ce-MoS_2 NSs have also been prepared. Fig. 3a shows the TEM image of Ag-MoS_2 NSs. The Ag NCs have a homogeneous distribution on the surface of ce-MoS_2 NSs with diameter about 9 nm. The lattice fringe about 0.205 nm can be assigned to (200) plane of Ag (JCPDS No. 87-0720). Pd NCs have relative larger size to Ag-MoS_2 with average size about 15 nm. Fig. 3e shows the HRTEM image of Pd NCs and the distinct lattice fringe about 0.225 nm owing to the (111) plane (JCPDS No. 89-4897). As shown in Fig. 3c, the Pt NCs can form either nanocrystals or superparticles. From the HRTEM image of Pt NCs shown in Fig. 3f, lattice spacing of 0.229 nm can be clearly observed, which can be assigned to (111) plane of Pt (JCPDS No. 87-0642). The formation of NM NCs on MoS_2 NSs has also been confirmed by EDS, as shown in Figure S3-S5.

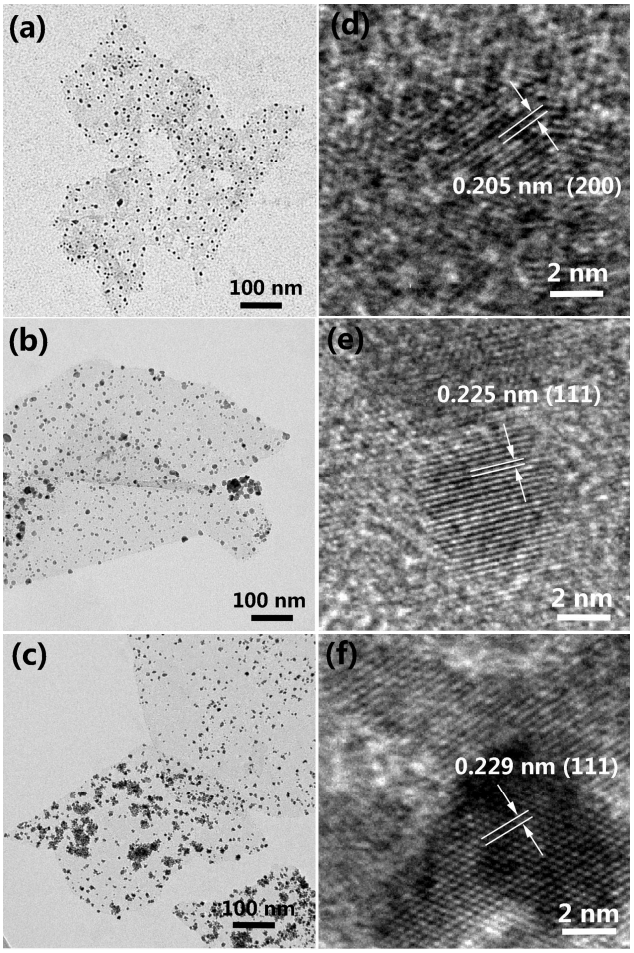

Fig. 3 (a)-(c) TEM images and (d)-(f) HRTEM images of Ag-MoS_2 NSs, Pd-MoS_2 NSs, and Pt-MoS_2 NSs, respectively.

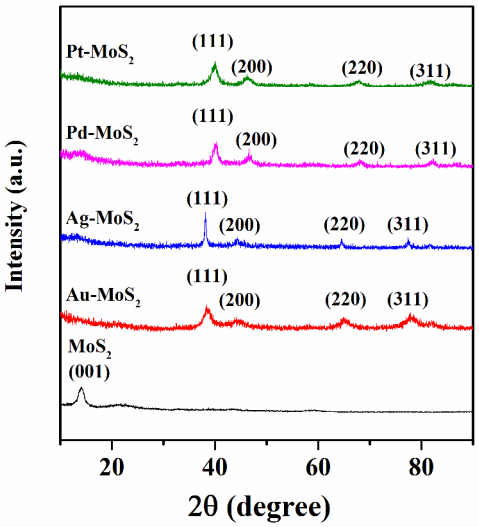

Fig. 4 XRD patterns of ce-MoS_2 NSs and NM-MoS_2 NSs (from bottom to top: Au-MoS_2, Ag-MoS_2 , Pd-MoS_2, and Pt-MoS_2)

Powder X-ray diffraction (XRD) was used to characterize the

structure of ce-MoS_2 NSs and NM-MoS_2 NSs. As shown in Fig. 4, the evident diffraction peak located at about 14.0° matches (001) index of 1T-MoS_2 as reported before.[20, 52] Broadened (001) peak suggests the ce-MoS_2 NSs are thin layers. Since (103) and (105) lines are strong diffraction peaks for 2H-MoS_2 phase, hence absence of both of them in the XRD pattern is another evidence for 1T-MoS_2 phase.[27, 52] After noble metal NCs modification, strong diffraction peaks emerge at 38.5°, 38.1°, 40.3°, and 40.0° from four different NM-MoS_2 NSs samples, which can be identified to the (111) planes of cubic Au (JCPDS No. 89-3697), Ag (JCPDS No. 87-0720), Pd (JCPDS No. 89-4897), and Pt (JCPDS No. 87-0642), respectively, indicating the successful formation of NM-MoS_2 NSs. The peak intensity of (001) plane of MoS_2 in NM-MoS_2 materials is much weaker than ce-MoS_2 NSs, which indicates surface modification by NM NCs can effectively separate the MoS_2 layers and suppress the ordered restacking process of the ce-MoS_2 NSs.[20]

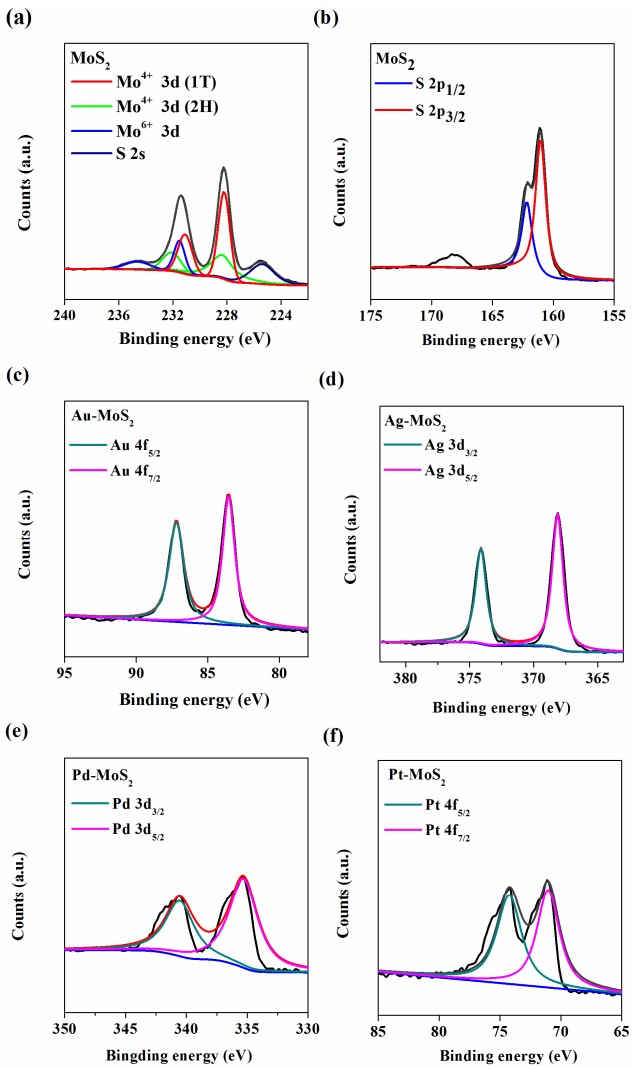

Fig. 5 XPS spectra of ce-MoS_2 NSs (a, b) and NM-MoS_2 NSs (from c to e: Au-MoS_2, Ag-MoS_2, Pd-MoS_2, and Pt-MoS_2).

Since the lithium intercalation-exfoliation process can alter the symmetry elements of S atoms and Mo atoms from trigonal prismatic (2H) to octahedral (1T) configuration, the binding energy of Mo 3d electrons change at the same time.[28, 52] XPS was carried out to investigate the structure and composition of ce-MoS_2 NSs and NM-MoS_2 NSs. As shown in Fig. 5a, by carefully deconvolution of the original spectra, the peaks of binding energy (BE) ranging from 220 eV to 240 eV can be fitted into four groups: (1) The doublet peaks located near 232 eV and 229 eV belong to Mo^{4+} $3d_{3/2}$ and Mo^{4+} $3d_{5/2}$ of 2H-MoS_2; (2) The doublet peaks located around 231 eV and 228 eV with relative lower BE can be assigned to Mo^{4+} $3d_{3/2}$ and Mo^{4+} $3d_{5/2}$ of 1T-MoS_2; (3) Relative weak peaks located at 235 eV and 231 eV are sign of Mo 3d peaks with higher oxidation state (Mo^{6+}), which may originate from the partial oxidation of Mo atoms at the edges or defects on the crystal plane of ce-MoS_2 NSs during chemical exfoliation; (4) The singlet S 2s peak locates at about 226 eV.[28, 37, 53] From the relative area of Mo^{4+} 3d peaks of 1T and 2H phases, we can infer that 1T is the mainly phase of ce-MoS_2 NSs. S 2p peaks of ce-MoS_2 NSs can be observed from Fig. 5b, accompanied with small peaks at about 168 eV from sulfur oxide, which may be introduced during the sample preparation.

Fig. 5c to Fig. 5f provides the binding energies of four different noble metals in NM-MoS_2 NSs. Peaks located at about 87.2 eV and 83.5 eV can be ascribed to Au $4f_{5/2}$ and Au $4f_{7/2}$, respectively; Peaks near 374.2 eV and 368.1 eV belong to Ag $3d_{3/2}$ and Ag $3d_{5/2}$, respectively; Peaks of Pd $3d_{3/2}$ and Pd $3d_{5/2}$ are near 340.6 eV and 335.4 eV, respectively; Peaks at 74.3 eV and 71.0 eV originate from Pt $4f_{5/2}$ and Pt $4f_{7/2}$, respectively.[53] Fig.5c-f suggest the successful deposition of different noble metals onto the surface of ce-MoS_2 NSs. On the other side, no obvious shift of the binding energies of Mo 3d and S 2p can be seen (data not shown), indicating that during surface modification process no oxidization happens to ce-MoS_2 NSs.

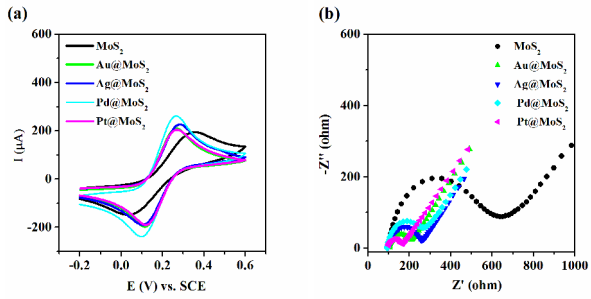

Fig. 6 Cyclic voltammetry (CV) curves (a) and impedance spectra (b) of ce-MoS_2 NSs and NM-MoS_2 NSs modified GCE in 0.1 M PBS containing 5 mM $Fe(CN)_6^{3-/4-}$.

Cyclic voltammetry was used to study the electrochemical properties of ce-MoS_2 NSs and NM-MoS_2 NSs. Different glassy carbon electrodes (GCEs) modified with ce-MoS_2 NSs (MoS_2-GCE) and NM-MoS_2 NSs (NM-MoS_2-GCE) were investigated in 0.1 M PBS (phosphate buffered saline) containing 5 mM $[Fe(CN)_6]^{3-/4-}$ with scanning rate of 100 mV/s. As shown in Fig. 6a, MoS_2-GCE shows reversible redox peaks with peak-to-peak separation (ΔE_p) about 308 mV. The redox peaks of NM-MoS_2-GCE are well-defined and the ΔE_p is about 160 mV, 170 mV, 170 mV, and 150 mV for Au-MoS_2-GCE, Ag-MoS_2-GCE, Pd-MoS_2-GCE, and Pt-MoS_2-GCE, respectively, which indicates that NM NCs modification can further improve the electron transfer capability of ce-MoS_2 NSs. Electrochemical impedance spectroscopy (EIS) was used to measure the charge-transfer

resistance (R_{ct}) of the NM-MoS_2 NSs modified GCEs. As illustrated in Fig. 6b, the R_{ct} of MoS_2-GCE is about 537 Ω and further decreases to 100 Ω, 160 Ω, 176 Ω, and 156 Ω, for Au-MoS_2-GCE, Ag-MoS_2-GCE, Pd-MoS_2-GCE, and Pt-MoS_2-GCE, respectively.

In order to further explore the potential of NM-MoS_2 NSs as electrocatalyst, we selected Pd-MoS_2 NSs to study their catalytic activity for methanol oxidation. As we know, although Pt is currently the most efficient catalyst for direct methanol fuel cells (DMFCs),[54-55] the limited reserve and high price hamper its industrial application.[56-57] As a low-cost and methanol-tolerant alternative for DMFCs, Pd catalysts have attracted much attention and great efforts have been carried out to design and synthesis novel nanostructured Pd catalysts.[57-58]

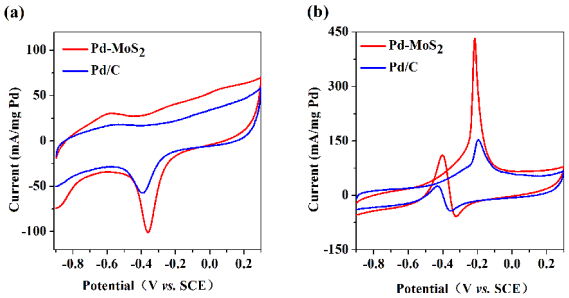

Fig. 7 Cyclic voltammograms of Pd-MoS_2 and Pd/C modified GCE in N_2-saturated 0.5 M KOH solution (a) and in N_2-saturated 0.5 M KOH + 1.0 M methanol solution (b) at scanning rate of 100 mV/s.

CV was carried out to evaluate the electrochemical activity of GCEs modified with Pd-MoS_2 NSs and Pd/C (10 wt%) in alkaline solution. Fig. 7a shows the CV curves of Pd-MoS_2 NSs and commercial Pd/C catalyst in N_2-saturated 0.5 M KOH solution at the scanning rate of 100 mV/s. The distinct cathodic peaks located near -0.4 V can be assigned to the reduction of palladium oxide.[59-60] Fig. 7b shows CVs of Pd-MoS_2 NSs and Pd/C modified GCEs in N_2-saturated electrolytes containing 0.5 M KOH + 1.0 M methanol. The CV curves show two peaks: one in the forward scan located at about -0.2 V is attributed to the direct oxidation of methanol molecules absorbed on the electrode surface, and the other peak in the reverse scan located at about -0.45 V can be assigned to the removal of carbonaceous species not completely oxidized in the forward scan.[59, 61] In order to compare the electrocatalytic activity of the catalysts, the anodic peak current for methanol oxidation was normalized to the mass of Pd element (the mass concentration of Pd in Pd-MoS_2 NSs was determined by ICP-OES). As shown in Fig. 7b, anodic peak current mass density of Pd-MoS_2 NSs is 433.5 mA/mg, about 2.8-fold to Pd/C catalyst (154.2 mA/mg), suggesting that Pd-MoS_2 NSs have much higher catalytic activity than Pd/C catalyst for methanol oxidation in alkaline media. Moreover, the SEM images (Figure S8) show that during the CV test the Pd nanoparticles keep stable and no obvious aggregation can be found.

As discussed above, 1T metallic phase in ce-MoS_2 NSs can significantly enhance the conductivity and lower the charge-transfer resistance, which is essential for high catalytic activity and may play an important role for the high catalytic activity of methanol oxidation. The R_{ct} of Pd-MoS_2 NSs is much smaller than Pd/C under the same conditions, as shown in Figure S6. In order to further investigate the influence of the 1T phase of MoS_2 on the catalytic activity of Pd-MoS_2, the electrochemical properties of Pd-MoS_2 before and after annealing were studied. Several previous studies have already shown that 1T phase MoS_2 is metastable and can be transformed to 2H phase by annealing,[27-28, 52] which has been used to study the catalytic activity of 1T and 2H MoS_2 for HER.[62] Similar experiments were performed and both of the catalytic activity and resistance of Pd-MoS_2 before and after annealing were studied. As shown in Figure S7a, after annealing at 300 □ for 1h under Ar atmosphere, the catalytic current for methanol oxidation decreases about 3 times from 48 μA to 16 μA. At the same time, the R_{ct} increases from 9 Ω to 56 Ω (Figure S7b). Since annealing at 300 □ for 1h can transfer most of the MoS_2 from 1T to 2H phase,[28] which significantly increases the resistance and lowers the catalytic current. Hence, 1T metallic phase of MoS_2 plays an important role in the high catalytic activity for methanol oxidation. On the other hand, homogeneously dispersed Pd NCs on ultrathin ce-MoS_2 NSs can improve their surface area, which may also contribute to the high catalytic activity.

Conclusions

In this study, we have developed a general and facile method to synthesize noble metal NCs modified ce-MoS_2 NSs in aqueous solution. Ultrathin ce-MoS_2 NSs was used as template to prepare series of NM-MoS_2 NSs, including Au, Ag, Pd, and Pt. Using CMC as stabilizer, noble metal NCs can be homogeneously deposited onto the surface of MoS_2 NSs to form water-dispersible NM-MoS_2 NSs. Since the chemical exfoliation method is very general to prepare different kinds of LTMDs NSs, hence, this synthetic strategy can be easily extended to prepare other NM-LTMDs NSs.

Optical and structural characterization indentified that the metallic 1T phase dominates the ce-MoS_2 NSs and effectively enhances its electrochemical property. Pd-MoS_2 NSs was studied as electrocatalyst for methanol oxidation and shows superior catalytic activity than commercial Pd/C catalyst, which was attributed to the metallic 1T phase of ce-MoS_2 NSs and the homogeneously deposition of Pd NCs on ce-MoS_2 NSs with large surface area.

Due to the existence of large numbers of LTMDs with various electrical properties, including semiconductors and semimetals,[4] noble metal modified chemically exfoliated LTMDs NSs stand for numerous promising candidates of advanced electrocatalysts not only for HER and methanol oxidation reaction, but also for other unexplored reactions.

Acknowledgements

This work was financially supported by the National Basic Research Program of China (2012CB933301), the Natural Science Foundation of Jiangsu Province (BK20130862), the Natural Science Foundation of Universities from Jiangsu Province (13KJB150029), the National Natural Science Foundation of China (21204038, 81273409), the Ministry of Education of China (IRT1148, 20123223110007), the Priority Academic Program Development of Jiangsu Higher Education Institutions (PAPD), the Open Research Fund of State Key Laboratory of Bioelectronics, Southeast University, and Starting Up Fund, Nanjing University of Posts & Telecommunications (NY211047).

Notes and references

[a] Institute of Advanced Materials (IAM), School of Materials Science and Engineering, and Key Laboratory for Organic Electronics & Information Displays (KLOEID), Nanjing University of Posts & Telecommunications, 9 Wenyuan Road, Nanjing, 210023, China.
[b] College of Geography and Biological Information, Nanjing University of Posts and Telecommunications, 9 Wenyuan Road, Nanjing, 210023, China.
* Authors to whom correspondence should be addressed;
Tel.: +86 25 85866333; Fax: +86 25 85866396.
E-mail: iamwhuang@njupt.edu.cn; iamlhwang@njupt.edu.cn;

[1] K. S. Novoselov, A. K. Geim, S. V. Morozov, D. Jiang, Y. Zhang, S. V. Dubonos, I. V. Grigorieva, A. A. Firsov, ***Science*** 2004**,** 306, 666.
[2] K. S. Novoselov, V. I. Falko, L. Colombo, P. R. Gellert, M. G. Schwab, K. Kim, ***Nature*** 2012**,** 490, 192.
[3] Q. H. Wang, K. Kalantar-Zadeh, A. Kis, J. N. Coleman, M. S. Strano, ***Nat. Nanotechnol.*** 2012**,** 7, 699.
[4] M. Chhowalla, H. S. Shin, G. Eda, L.-J. Li, K. P. Loh, H. Zhang, ***Nat. Chem.*** 2013**,** 5, 263.
[5] X. Huang, Z. Zeng, H. Zhang, ***Chem. Soc. Rev.*** 2013**,** 42, 1934.
[6] M. Xu, T. Liang, M. Shi, H. Chen, ***Chem. Rev.*** 2013**,** 113, 3766.
[7] J. A. Wilson, A. D. Yoffe, ***Adv. Phys.*** 1969**,** 18, 193.
[8] M. Stefanov, A. N. Enyashin, T. Heine, G. Seifert, ***J. Phys. Chem. C*** 2008**,** 112, 17764.
[9] T. F. Jaramillo, K. P. Jørgensen, J. Bonde, J. H. Nielsen, S. Horch, I. Chorkendorff, ***Science*** 2007**,** 317, 100.
[10] E. Gourmelon, O. Lignier, H. Hadouda, G. Couturier, J. C. Bernède, J. Tedd, J. Pouzet, J. Salardenne, ***Sol. Energy Mater. Sol. Cells*** 1997**,** 46, 115.
[11] D. Chadwick, M. Breysse, ***J. Catal.*** 1981**,** 71, 226.
[12] R. Coehoorn, C. Haas, J. Dijkstra, C. J. F. Flipse, R. A. de Groot, A. Wold, ***Phys. Rev. B*** 1987**,** 35, 6195.
[13] C. B. Roxlo, R. R. Chianelli, H. W. Deckman, A. F. Ruppert, P. P. Wong, ***J. Vac. Sci. Technol., A*** 1987**,** 5, 555.
[14] K. F. Mak, C. Lee, J. Hone, J. Shan, T. F. Heinz, ***Phys. Rev. Lett.*** 2010**,** 105, 136805.
[15] A. Splendiani, L. Sun, Y. B. Zhang, T. S. Li, J. Kim, C. Y. Chim, G. Galli, F. Wang, ***Nano. Lett.*** 2010**,** 10, 1271.
[16] B. Radisavljevic, A. Radenovic, J. Brivio, V. Giacometti, A. Kis, ***Nat. Nanotechnol.*** 2011**,** 6, 147.
[17] O. Lopez-Sanchez, D. Lembke, M. Kayci, A. Radenovic, A. Kis, ***Nat. Nanotechnol.*** 2013**,** 8, 497.
[18] K. Novoselov, D. Jiang, F. Schedin, T. Booth, V. Khotkevich, S. Morosov, A. Geim, ***Proc. Nat. Acad. Sci.*** 2005**,** 102, 10454.
[19] J. N. Coleman, M. Lotya, A. O'Neill, S. D. Bergin, P. J. King, U. Khan, K. Young, A. Gaucher, S. De, R. J. Smith, et al., ***Science*** 2011**,** 331, 568.
[20] P. Joensen, R. F. Frindt, S. R. Morrison, ***Mater. Res. Bull.*** 1986**,** 21, 457.
[21] Z. Zeng, Z. Yin, X. Huang, H. Li, Q. He, G. Lu, F. Boey, H. Zhang, ***Angew. Chem. Int. Ed.*** 2011**,** 50, 11093.
[22] Z. Zeng, T. Sun, J. Zhu, X. Huang, Z. Yin, G. Lu, Z. Fan, Q. Yan, H. H. Hng, H. Zhang, ***Angew. Chem. Int. Ed.*** 2012**,** 51, 9052.
[23] Y.-H. Lee, X.-Q. Zhang, W. Zhang, M.-T. Chang, C.-T. Lin, K.-D. Chang, Y.-C. Yu, J. T.-W. Wang, C.-S. Chang, L.-J. Li, et al., ***Adv. Mater.*** 2012**,** 24, 2320.
[24] K.-K. Liu, W. Zhang, Y.-H. Lee, Y.-C. Lin, M.-T. Chang, C.-Y. Su, C.-S. Chang, H. Li, Y. Shi, H. Zhang, et al., ***Nano. Lett.*** 2012**,** 12, 1538.
[25] H. Matte, A. Gomathi, A. K. Manna, D. J. Late, R. Datta, S. K. Pati, C. N. R. Rao, ***Angew. Chem. Int. Ed.*** 2010**,** 49, 4059.
[26] S. Jeong, D. Yoo, J.-t. Jang, M. Kim, J. Cheon, ***J. Am. Chem. Soc.*** 2012**,** 134, 18233.
[27] F. Wypych, R. Schollhorn, ***J. Chem. Soc., Chem. Commun.*** 1992, 1386.
[28] G. Eda, H. Yamaguchi, D. Voiry, T. Fujita, M. Chen, M. Chhowalla, ***Nano. Lett.*** 2011**,** 11, 5111.
[29] M. A. Lukowski, A. S. Daniel, F. Meng, A. Forticaux, L. Li, S. Jin, ***J. Am. Chem. Soc.*** 2013**,** 135, 10274.
[30] D. Voiry, H. Yamaguchi, J. Li, R. Silva, D. C. B. Alves, T. Fujita, M. Chen, T. Asefa, V. B. Shenoy, G. Eda, et al., ***Nat. Mater.*** 2013**,** 12, 850.
[31] P. K. Jain, X. Huang, I. H. El-Sayed, M. A. El-Sayed, ***Acc. Chem. Res.*** 2008**,** 41, 1578.
[32] P. Herves, M. Perez-Lorenzo, L. M. Liz-Marzan, J. Dzubiella, Y. Lu, M. Ballauff, ***Chem. Soc. Rev.*** 2012**,** 41, 5577.
[33] Y. Liang, Y. Li, H. Wang, H. Dai, ***J. Am. Chem. Soc.*** 2013**,** 135, 2013.
[34] C. Tan, X. Huang, H. Zhang, ***Mater. Today*** 2013**,** 16, 29.
[35] W. Xu, X. Ling, J. Xiao, M. S. Dresselhaus, J. Kong, H. Xu, Z. Liu, J. Zhang, ***Proc. Nat. Acad. Sci.*** 2012**,** 109, 9281.
[36] J.-K. Lee, W. Lee, T.-J. Yoon, G.-S. Park, J.-H. Choy, ***J. Mater. Chem.*** 2002**,** 12.
[37] X. Huang, Z. Zeng, S. Bao, M. Wang, X. Qi, Z. Fan, H. Zhang, ***Nat. Commun.*** 2013**,** 4, 1444.
[38] J. Kim, S. Byun, A. J. Smith, J. Yu, J. Huang, ***J. Phys. Chem. Lett.*** 2013**,** 4, 1227.
[39] D. Martin B, ***Mater. Res. Bull.*** 1975**,** 10, 287.
[40] J. Liu, J. Sutton, C. B. Roberts, ***J. Phys. Chem. C*** 2007**,** 111, 11566.
[41] Liu, F. He, E. Durham, D. Zhao, C. B. Roberts, ***Langmuir*** 2007**,** 24, 328.
[42] J. Tan, R. Liu, W. Wang, W. Liu, Y. Tian, M. Wu, Y. Huang, ***Langmuir*** 2010**,** 26, 2093.
[43] S. Magdassi, A. Bassa, Y. Vinetsky, A. Kamyshny, ***Chem. Mater.*** 2003**,** 15, 2208.
[44] O.-K. Kim, J. Je, J. W. Baldwin, S. Kooi, P. E. Pehrsson, L. J. Buckley, ***J. Am. Chem. Soc.*** 2003**,** 125, 4426.
[45] Q. Yang, X. Pan, F. Huang, K. Li, ***J. Phys. Chem. C*** 2010**,** 114, 3811.
[46] J. P. Wilcoxon, P. P. Newcomer, G. A. Samara, ***J. Appl. Phys.*** 1997**,** 81, 7934.
[47] Z. Zhang, F. Xu, W. Yang, M. Guo, X. Wang, B. Zhang, J. Tang, ***Chem. Commun.*** 2011**,** 47, 6440.
[48] T. Teranishi, M. Miyake, ***Chem. Mater.*** 1998**,** 10, 594.
[49] S.-Y. Zhao, S.-H. Chen, S.-Y. Wang, D.-G. Li, H.-Y. Ma, ***Langmuir*** 2002**,** 18, 3315.
[50] Y. Shi, J.-K. Huang, L. Jin, Y.-T. Hsu, S. F. Yu, L.-J. Li, H. Y. Yang, ***Sci. Rep.*** 2013**,** 3, 1839.
[51] W. M. R. Divigalpitiya, R. F. Frindt, S. R. Morrison, ***Science*** 1989**,** 246, 369.
[52] M. A. Py, R. R. Haering, ***Can. J. Phys.*** 1983**,** 61, 76.
[53] B. V. Crist, ***Handbook of Monochromatic XPS Spectra, Wiley-VCH,*** 1999.

[54] A. S. Arico, S. Srinivasan, V. Antonucci, ***Fuel Cells*** 2001**,** 1, 133.
[55] H. S. Liu, C. J. Song, L. Zhang, J. J. Zhang, H. J. Wang, D. P. Wilkinson, ***J. Power Sources*** 2006**,** 155, 95.
[56] E. Antolini, E. R. Gonzalez, ***J. Power Sources*** 2010**,** 195, 3431.
[57] X. Zhao, M. Yin, L. Ma, L. Liang, C. Liu, J. Liao, T. Lu, W. Xing, ***Energy Environ. Sci.*** 2011**,** 4, 2736.
[58] C. Bianchini, P. K. Shen, ***Chem. Rev.*** 2009**,** 109, 4183.
[59] R. N. Singh, A. Singh, Anindita, ***Int. J. Hydrogen Energy*** 2009**,** 34, 2052.
[60] H. Huang, X. Wang, ***J. Mater. Chem.*** 2012**,** 22, 22533.
[61] C. Xu, L. Cheng, P. Shen, Y. Liu, ***Electrochem. Commun.*** 2007**,** 9, 997.
[62] D. Voiry, M. Salehi, R. Silva, T. Fujita, M. Chen, T. Asefa, V. B. Shenoy, G. Eda, M. Chhowalla, ***Nano. Lett.*** 2013**,** 13, 6222.

Table of contents entry

Noble metal nanoparticles modified MoS_2 nanosheets were prepared and Pd-MoS_2 was explored as enhanced electrocatalyst for methanol oxidation.